ELSEVIER

Contents lists available at ScienceDirect

Commun Nonlinear Sci Numer Simulat

journal homepage: www.elsevier.com/locate/cnsns



Short communication

Mapping recovery from sleep deprivation

Sofia H. Piltz^a, Christina Athanasouli^a, Cecilia G. Diniz Behn^{b,c}, Victoria Booth^{a,d,*}

- ^a Department of Mathematics, University of Michigan, 530 Church Street, Ann Arbor, MI, 48109-1043, USA
- ^b Department of Applied Mathematics and Statistics, Colorado School of Mines, 1500 Illinois Street, Golden, CO, 80401, USA
- ^c Department of Pediatrics, University of Colorado Anschutz Medical Campus, 13001 East 17th Place, Aurora, CO, 80045, USA
- d Department of Anesthesiology, University of Michigan, 1500 E Medical Center Drive, Ann Arbor, MI, 48109-5048, USA



ARTICLE INFO

Article history:
Received 2 September 2020
Accepted 22 December 2020
Available online 29 December 2020

MSC: 34C60 92B25

Keywords:
One-dimensional maps
Discontinuous maps
Ordinary differential equations
Sleep deprivation
Circadian rhythm

ABSTRACT

Sleep timing is based on the interactions between circadian and homeostatic processes. However, sleep deprivation perturbs the time of sleep onset, and the timing and duration of the following recovery sleep may differ from that of baseline sleep. Here we show that the responses to 0-24 h of sleep deprivation can be approximated by a one-dimensional. discontinuous map computed from a physiologically-based ordinary differential equation model for human sleep-wake regulation. The map relates the circadian phase of sleep onset to the circadian phase of the previous sleep onset and reproduces sleep patterns seen in experimental data for the timing and duration of recovery sleep when sleep onset occurs 8 or 20 h after the usual sleep onset. In addition, the durations of recovery sleep predicted by the map for sleep deprivations of 0 to 24 h are consistent with numerical simulations of recovery sleep using the full (nonautonomous, 8-dimensional) model. Our results demonstrate that the circadian phase of sleep onset affects the duration of recovery sleep more strongly than the homeostatic sleep drive for most durations of sleep deprivation. In addition, the map establishes a lower bound for the length of recovery sleep. As a result, the map provides a computationally-efficient way of incorporating sleep dynamics into new technologies that allow users to predict the effects of sleep deprivation and identify optimal sleep schedules.

© 2020 Elsevier B.V. All rights reserved.

1. Introduction

The primary processes dictating the timing and duration of sleep and wake episodes are the *circadian* (i.e., approximately 24-hour) *rhythm* and the *homeostatic sleep drive* (i.e., the need for sleep that increases with time awake). Under typical adult human sleep-wake schedules, these two processes work together to promote consolidated waking during the day and consolidated sleep during the night. However, when sleep schedules are disrupted, for example due to sleep deprivation, these processes may compete and affect the timing and duration of sleep episodes. For example, recovery sleep following sleep deprivation may be shorter or longer than habitual sleep duration depending on the circadian phase (time of day) of the onset of recovery sleep [1]. Furthermore, while nocturnal sleep typically includes both rapid eye movement (REM) and

^{*} Corresponding author at: Department of Mathematics, University of Michigan, 530 Church Street, Ann Arbor, MI, 48109-1043, USA. *E-mail address:* vbooth@umich.edu (V. Booth).

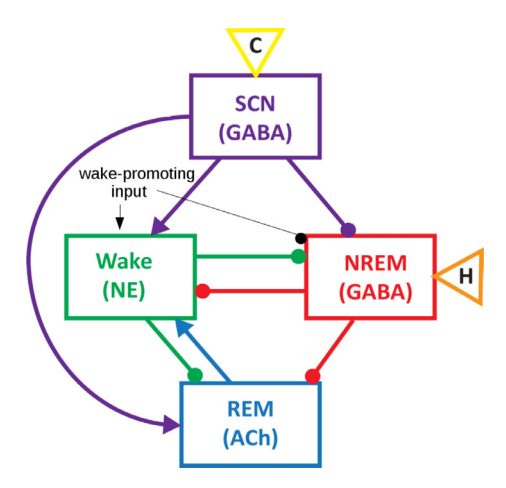


Fig. 1. Model schematic. The physiologically-based model [20] for human sleep incorporates equations for the average firing rate of the neuronal populations promoting states of Wake, NREM and REM sleep, and the SCN (boxes; NE, GABA, and ACh indicate the primary neurotransmitters for each population), the homeostatic sleep drive (*H*, orange triangle), and the circadian clock oscillator (*C*, yellow triangle). Excitatory (inhibitory) effects of neurotransmittermediated projections among populations are indicated by arrows (circles). To simulate sleep deprivation, we impose a wake-promoting input (black) that is excitatory to the wake population and inhibitory to the NREM sleep population. (For interpretation of the references to color in this figure legend, the reader is referred to the web version of this article.)

non-REM (NREM) sleep states, with cyclic alternation between the two states over the course of the night, sleep deprivation may affect the duration and timing of both NREM and REM sleep [2].

Mathematical models of sleep-wake regulation have been previously used to understand and predict changes in sleep not only after sleep deprivation but also as a result of other perturbations including shift work, travel across time zones, sleep disorders such as narcolepsy, and pharmacological interventions [3–7]. While the classic two-process model [8,9] accounts for sleep deprivation by considering interactions between the homeostatic sleep drive (Process S) and the circadian rhythm (Process C) [3,10], more recent physiologically-based models consider the effects of extended wakefulness on connections between neuronal populations that govern sleep-wake dynamics [11–14]. In previous work, we used a physiologically-based model that includes wake and both NREM and REM sleep states, as well as the circadian rhythm, to investigate the variation of sleep deprivation responses in individuals with different habitual sleep durations (e.g., long and short sleepers) [15].

Previously, it has been shown that the solutions to the two-process model can be represented with a one-dimensional circle map that establishes the relationship between the circadian phases of two consecutive sleep onsets [16–19]. These maps feature discontinuities (e.g., vertical gaps) caused by competition between the circadian rhythm and the homeostatic sleep drive in determining sleep and wake durations. We have shown that the solutions to our physiologically-based sleep-wake network model [20] can be represented by a numerically-computed, one-dimensional map [21]. In addition to the gaps found in maps for models that describe only wake and sleep states, this map exhibits multiple gaps with distinct branches of the map corresponding to sleep episodes with different numbers of REM bouts. Here, we apply this map [21] to predict responses to sleep deprivation and validate these results with both experimental data and numerical simulations of the model [20] that incorporate behaviorally-appropriate light schedules.

This paper is organized as follows. In Section 2, we first review the equations of the 8-dimensional ordinary differential equation model for human sleep-wake dynamics and then summarize the numerical computation of the map representing the dynamics of the model in Section 2.2. In addition, we decompose the map and use it to compute the length of recovery sleep following sleep deprivation. In Section 3, we present predictions obtained from the map for (i) the length and (NREM-REM) composition of recovery sleep and (ii) the duration of recovery sleep from 0 to 24 h of sleep deprivation. Furthermore, we compare these predictions with experimental data and numerical simulations of the full model. Finally, we discuss our findings and their implications in Section 4.

2. Methods

2.1. Physiologically-based model for human sleep and wake dynamics

The sleep-wake regulatory network model [20] is based on current hypotheses for the interactions of hypothalamic and brainstem neural populations that influence the behavioral state (see Fig. 1). The model includes connections among neuronal populations that have been identified as promoting wake (W), non-REM (NREM) sleep, and REM (REM) sleep states, a suprachiasmatic nucleus population (SCN) that propagates the intrinsic circadian rhythm (C) to the neuron populations, and the homeostatic sleep drive variable (H) which modulates activity of the NREM population (Fig. 1). Four of the system variables correspond to the mean firing rates (in Hz) of neuron populations active during wake, NREM sleep, REM sleep, and

of the SCN, $F_X(t)$ (X = Wake, NREM, REM and SCN), with the rate of change of F_X dictated by:

$$\dot{F}_{X} = \frac{F_{X\infty}[\sum_{i} g_{i,X} R_{i\infty}(F_{Yi})] - F_{X}}{\tau_{Y}}, \qquad (2.1)$$

where $F_{X\infty}[\cdot]$ is the firing rate response function, $g_{i,X}$ is a non-dimensional weight parameter, $R_{i\infty}$ is the neurotransmitter release function, and τ_X is the time scale at which $F_X(t)$ evolves. When $g_{i,X} > 0$ ($g_{i,X} < 0$), the presynaptic neuronal population Y (Y =Wake, NREM, REM and SCN) excites (inhibits) population X. The function $F_{X\infty}[r]$, which for X =Wake, NREM and REM takes a weighted sum of neurotransmitter concentrations (released because of the activity in presynaptic neuronal populations) as its argument, has a sigmoidal form and saturates for high levels of neurotransmitter r:

$$F_{X\infty}[r] = \frac{X_{\text{max}}}{2} \left(1 + \tanh[(r - \beta_X)/\alpha_X] \right), \tag{2.2}$$

where X_{max} is the maximum firing rate, α_X is the sensitivity of the response, and β_X is the half-activation threshold of population X. The neurotransmitter concentration released as a result of activity of the presynaptic neuronal population depends on the mean firing rate of the presynaptic neuronal population F_Y . This dependency is determined by the steady state neurotransmitter release function, $R_{i\infty}(f)$ (i = NE, GABA, and ACh), for a presynaptic firing rate f as follows:

$$R_{i\infty}(f) = \tanh(f/\gamma_i), \tag{2.3}$$

where γ_i is the sensitivity of the release. This represents a reduced version of the model [15,20] in which we make the simplifying assumption of instantaneous neurotransmitter release by the presynaptic neuronal population, that is, $\dot{F}_{\chi} \ll \dot{R}_i$. This simplification reduces the dimensionality of the model and does not qualitatively affect model dynamics [22].

Circadian variation of the firing rate of the SCN population is driven by the circadian clock oscillator, C(t), which is the only argument of the SCN firing rate response function $F_{SCN\infty}[r]$ in Eq. (2.1). Biologically, C(t) can be considered as the 24-hour rhythm observed in human circadian markers, such as body temperature. The dynamics of C(t) are described by the human circadian clock model fitted to experimental data describing circadian responses to light [23,24]. Using published parameter values [23,25], the model generates oscillations in C that drive the average firing rate of the SCN population, F_{SCN} , between 1 and 7 Hz [26]. Under regular conditions, we simulate a 14-hour:10-hour environmental light:dark cycle with light intensity I = 5000:I = 0 lux. In simulations of sleep deprivation (see Figs. 2, 4, and 5), we mimic the light environment used in experimental sleep deprivation studies (e.g., [10]). That is, if the model's state is "awake" during the environmental dark period, I = 300 lux to represent indoor light intensity for light activity such as reading. By contrast, if the model is "asleep" during the environmental light period, I = 100 lux to represent light penetrating the eyelids.

Activity of the NREM population is influenced by the homeostatic sleep drive, H(t), and the dynamics of H(t) reflect the dynamics of the established marker of sleep homeostasis, the power of slow wave activity (SWA) (i.e., EEG power in the range between 0.75 and 4.5 Hz) during slow wave sleep [27]. The dynamics of H(t) are given by the following equation

$$\dot{H} = \frac{(H_{\text{max}} - H)}{\tau_{Hw}} \mathcal{H}[F_W - \theta_W] - \frac{H}{\tau_{Hs}} \mathcal{H}[\theta_W - F_W], \qquad (2.4)$$

where \mathcal{H} is a Heaviside function¹, H_{max} is the maximum % of the mean SWA, and τ_{Hw} and τ_{Hs} are the time constants for the exponential increase during wake and decrease during sleep in the power of the SWA, respectively. These three parameters are specified based on experimental results of EEG recordings in humans [27]. We assume that the state of decrease (sleep) or increase (wake) of the homeostatic sleep drive is governed by the mean firing rate of the wake population. That is, the homeostatic sleep drive starts to increase (decrease), and the model is in wake (sleep) state, when F_W crosses its threshold value θ_W from below (above). H influences the transitions between wake and sleep states through its modulation of the excitability of the firing rate response function of the NREM population, $F_{NREM\infty}[\cdot]$. Specifically, a large H value decreases the half-activation threshold as follows: $\beta_{NREM}(H) = -0.0045H - b_{H\beta}$.

We use values of model parameters identifed in previous work [15] where we computed an ensemble of about 20,000 parameter sets that were fit to replicate the baseline wake, REM and NREM sleep timing and durations experimentally measured from humans exhibiting typical (and habitual) sleep behavior [28]. Results shown here were derived using a parameter set corresponding to median values of the ensemble, with variability between the 25th and 75th percentile values of the ensemble shown in Figs. 3, 4 and 6. For a complete list of the model equations and parameter values, see [15].

Time traces of the activity of the neuronal populations (top), H (middle), and C (bottom) for two example simulations of sleep deprivation where sleep onset occurs 8 and 20 h past the usual sleep onset (indicated by a vertical dotted line) are shown in Fig. 2, panels A and C, respectively. Because the homeostatic sleep drive and the circadian rhythm vary more slowly than the transitions between states, we consider a fast-slow decomposition of the dynamics of the model by taking H and C as fixed parameters [22]. This reveals a 3-dimensional surface of steady state solutions where the top (blue) manifold indicates the stable steady "wake" state and the bottom (red) manifold indicates an unstable steady state associated with the stable periodic solution representing NREM-REM cycling during the "sleep" state (Fig. 2B and D). The manifold in the middle (gray) is the unstable steady state dividing the basins of attraction of the "wake" and "sleep" states, and the solid black curves (where the blue and gray (gray and red) manifolds coalesce) denote saddle-node bifurcation points. When H

¹ That is, $\mathcal{H}[z] = 0$ if z < 0 and $\mathcal{H}[z] = 1$ if $z \ge 0$.

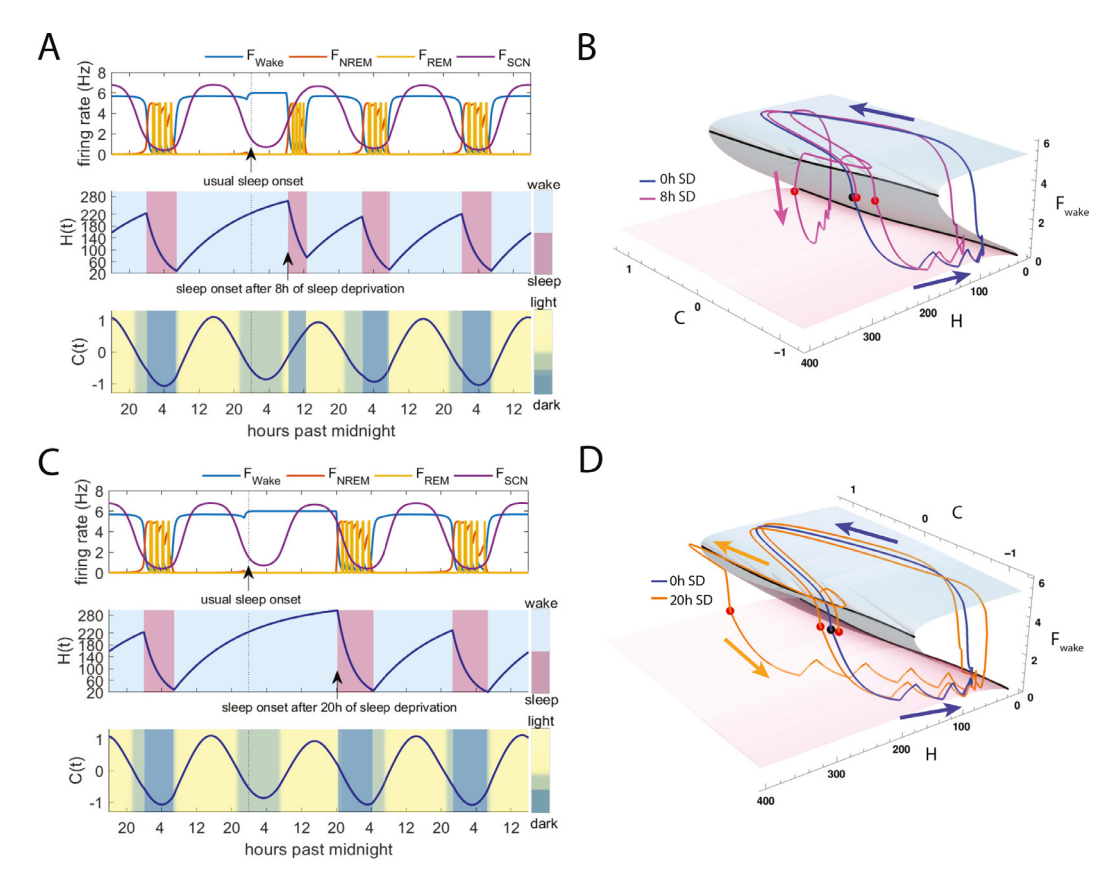


Fig. 2. Example model simulations for sleep deprivation of 8 and 20 h. A,C: Time traces of population firing rates (top), homeostatic sleep drive H (middle) and circadian drive C (bottom) for four days with sleep deprivation of 8h (A) and 20h (C) from usual sleep onset occurring on the 2nd day (usual sleep onset indicated with black arrows and vertical dotted line). Light intensity input to the circadian clock oscillator varies with simulated model behavior (background colors in bottom panels, see also Section 2). **B,D:** Surface of steady state solutions revealed by a fast-slow decomposition of the model when *H* and *C* are taken as fixed parameters. The top (blue) surface represents the stable wake state and the bottom (red) surface represents the unstable solution surrounded by the stable periodic solution (e.g., see blue trajectory) exhibiting NREM-REM cycles. Trajectories for the full model when *H* and *C* are allowed to vary show how the steady state "wake" and "sleep" manifolds influence solutions of the full model [blue trajectory shows the stable, baseline sleep model solution while the purple (orange) trajectory is the model solution for 8 h (20 h) of sleep deprivation B (D)]. We indicate sleep onsets on the trajectories with filled circles. (For interpretation of the references to color in this figure legend, the reader is referred to the web version of this article.)

and C vary, model solution trajectories traverse the stable "wake" and "sleep" manifolds with transitions between states occurring as the trajectory passes over the curves of saddle node points (see the blue curve, where we indicate sleep onsets with circles and the oscillations in the trajectory along the lower red manifold reflect the occurrence of REM sleep episodes).

During simulations of sleep deprivation (purple and orange curves in Fig. 2B and D, respectively), the trajectory continues to evolve along the "wake" manifold, close to the curve of saddle-node points instead of dropping to the "sleep" state as occurs under typical sleep-wake conditions (black filled circles on blue trajectory in Fig. 2B and D). When sleep onset eventually occurs (leftmost purple and orange filled circles in Fig. 2B and D), the trajectories exhibit different paths on the "sleep" manifold than the baseline (blue) trajectory reflecting differences in sleep durations and timing. These perturbed trajectories obtain higher than baseline values in *H* as *H* increases during the extended "wake" state of the model (Fig. 2A and C, middle panels) and have slightly varied *C* values due to differences in light exposure (Fig. 2A and C, bottom panels). Over the following few sleep-wake cycles, these trajectories approach the baseline trajectory for the stable sleep-wake pattern (Fig. 2B and D).

2.2. One-dimensional maps and computing the length of sleep (wake) time

The dynamics of the sleep-wake model can be described by a one-dimensional map for successive circadian phases of sleep onset. The map represents the relationship between the sleep onset at a given circadian phase on the nth sleep cycle (consisting of one sleep and one wake episode) and the successive sleep onset, occurring on the n+1st sleep cycle. The map is computed numerically by simulating the model from initial conditions given by stable solutions of the neuronal population equations near the sleep onset points (see black curve on the blue manifold in Fig. 2C and D) associated with each

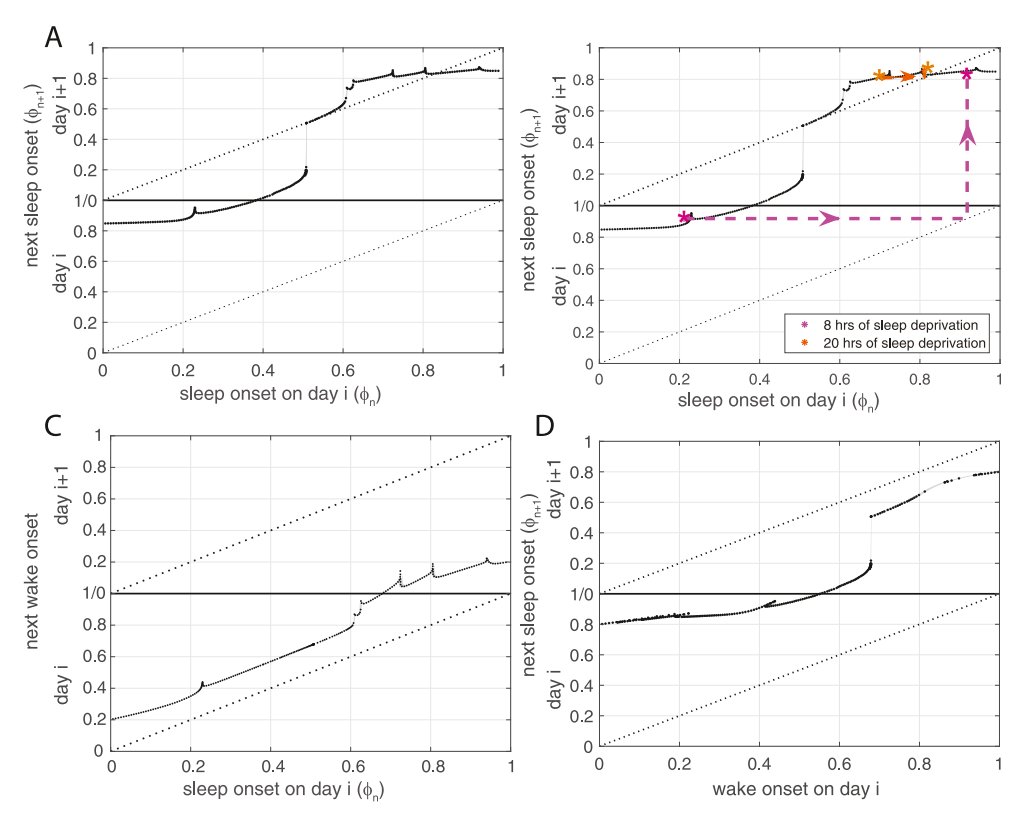


Fig. 3. One-dimensional maps representing the dynamics of the sleep-wake network model. A,B: Map Φ_{ss} gives the circadian phase of the n+1st sleep onset (ϕ_{n+1}) on day (circadian cycle) i (bottom panel) or i+1 (top panel) as a function of the circadian phase of the nth sleep onset on day (circadian cycle) i (ϕ_n). **B:** Cobwebbing of sleep onset phases during simulations of 8h (purple) and 20h (orange) of sleep deprivation as shown in Fig. 2. **C:** Map Φ_{sw} gives the circadian phase of the next wake onset [on day i (bottom) or i+1 (top)] as a function of the circadian phase of the nth sleep onset ϕ_n on day i. **D:** Map Φ_{ws} gives the circadian phase of the next sleep onset $[\phi_{n+1}]$ on day i (bottom) or i+1 (top)] as a function of the circadian phase of the wake onset on day i. Phase 0/1 indicates the minimum of the circadian variable i C. The black dots are map point values computed from the model using the median values of the parameter ensemble for typical adult sleep-wake behavior and the gray bands indicate variability in the maps computed using parameter values at the 25th and 75th percentile of the ensemble (for more details, see [15]). (For interpretation of the references to color in this figure legend, the reader is referred to the web version of this article.)

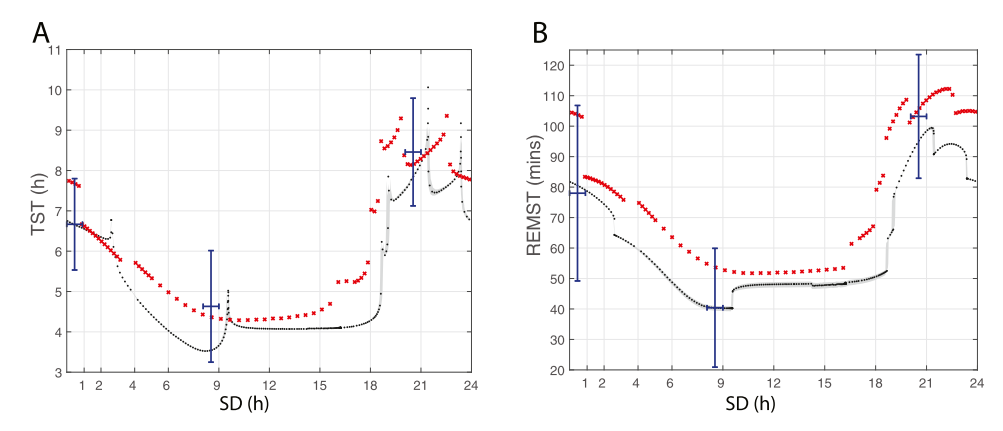


Fig. 4. Predicted durations of recovery sleep following 0-24 h of sleep deprivation. Comparison of the total sleep time (TST, A) and REM sleep time (REMST, B) predicted by the map Φ_{sw} for sleep onsets at circadian phases associated with 0 to 24h of sleep deprivation (SD) (i.e., sleep onset occurs 0-24h after the usual (baseline) sleep onset) (black dots and gray shading) and model simulations of 0 to 24h of sleep deprivation (red crosses). The model simulations are computed with median parameter values and the gray shading represents the 25th and 75th percentiles of the parameter ensemble (for more details, see [15]). Experimentally-measured durations of recovery TST and REMST for 0h, $\approx 8h$ and $\approx 20h$ of sleep deprivation have been reported in [28] (blue markers including \pm standard deviation for sleep onset phases and durations). (For interpretation of the references to color in this figure legend, the reader is referred to the web version of this article.)

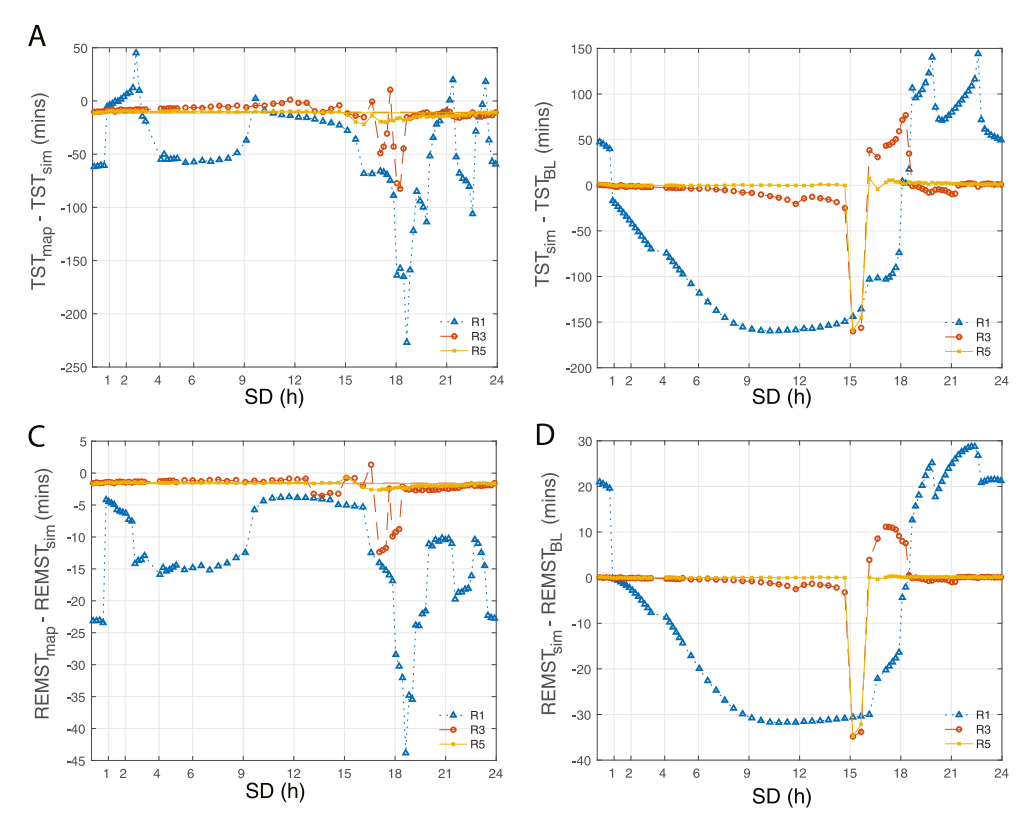


Fig. 5. Differences between predictions based on the map and model simulations. A,C: Difference in total sleep time (A) and REM sleep time (C) during the first (R1, blue triangles), third (R3, red circles) and fifth (R5, yellow crosses) recovery sleep episodes following 0 to 24h of sleep deprivation predicted by the map (TST_{map}, REMST_{map}) and by model simulations of sleep deprivation (TST_{sim}, REMST_{sim}). B,D: Difference between usual (baseline) TST (TST_{BL}, B) and (baseline) REMST (REM_{BL}, D) in the first (R1, blue triangles), third (R3, red circles) and fifth (R5, yellow crosses) recovery sleep episodes following 0 to 24h of sleep deprivation predicted by model simulations (TST_{sim}, REMST_{sim}). The *x*-axis indicates the sleep onset in 0–24h after the usual (baseline) sleep onset (SD). For panels A and C, the usual sleep onset is considered as the sleep onset of the fixed point of the map Φ_{ss}, while for panels C and D, the usual sleep onset is that of the stable periodic solution in the model simulations. We note that because of the differences in light schedules, there is a (negligible) difference between the circadian phase of the fixed point and that of the stable periodic solution. (For interpretation of the references to color in this figure legend, the reader is referred to the web version of this article.)

value of C such that the auxiliary circadian variables are assumed to be on their stable solution. For a detailed description of the algorithm, see [21]. When the model simulation is started from these (or nearby) initial values, the solution transitions quickly to the sleep state and the time (and circadian phase) of the next sleep onset can be collected by continuing the model simulation forward in time [21]. In order to maintain a consistent definition of circadian phase to compute the map, during the numerical simulations of the model the light cycle is fixed to the environmental 14:10h L:D cycle (i.e., I = 500 (I = 0) lux during the light (L) (dark, D) period as in [21]). This fixed light schedule used for computing the map contrasts with the behaviorally-gated light schedule used to simulate sleep deprivation in the full model where we mimic the light exposure schedules during the experimental conditions (see Section 2).

The one-dimensional map, Φ_{ss} , gives the circadian phase for sleep onset on sleep cycle n+1, ϕ_{n+1} , as a function of the circadian phase of sleep onset on sleep cycle n, ϕ_n (see Fig. 3A):

$$\phi_{n+1} = \Phi_{ss}(\phi_n). \tag{2.5}$$

The n+1st sleep onset may occur during the same circadian cycle as the nth sleep onset (day i in Fig. 3) or during the following circadian cycle (day i+1). In this work, we decompose Φ_{ss} into two maps (Fig. 3C and D, respectively): (1) Φ_{sw} which gives the circadian phase of wake onset as a function of the circadian phase of the preceding sleep onset and (2) Φ_{ws} which gives the circadian phase of sleep onset as a function of the circadian phase of the preceding wake onset at sleep cycle n. Thus,

$$\phi_{n+1} = \Phi_{ss}(\phi_n) = (\Phi_{ws} \circ \Phi_{sw})(\phi_n) = \Phi_{ws}[\Phi_{sw}(\phi_n)]. \tag{2.6}$$

Decomposing the sleep onset-sleep onset map Φ_{ss} into a composition of Φ_{ws} and Φ_{sw} allows us to determine the length of time asleep (awake) for a given sleep (wake) onset phase predicted by the map. Thus, if the phase of the next wake (sleep) onset is above the y = x -line, the time spent asleep (awake) is (in hours)

$$\Delta S = 24(y - x). \tag{2.7}$$

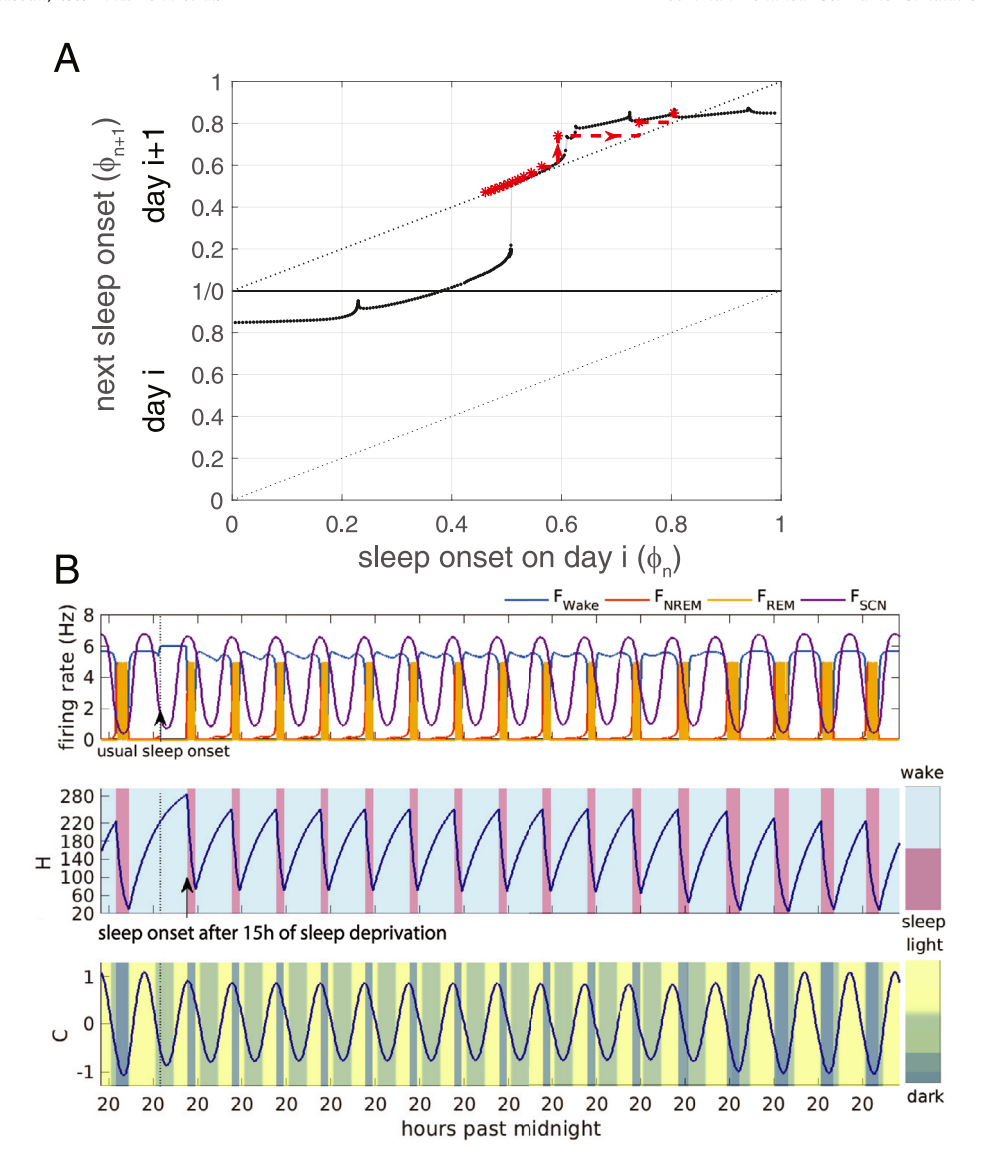


Fig. 6. An example of long-lasting effects of acute sleep deprivation A: A model simulation for approximately 15h of sleep deprivation (asterisks) generates an initial sleep onset near the region of the unstable fixed point of the map (black dots and gray shading). B: Similarly, simulation of the full model predicts a long transient (of about 12 days) before returning to the baseline sleep solution. During this transient, sleep episodes are short (about 2.7 h less than baseline sleep) and desynchronized from the circadian rhythm with sleep onsets occurring in the afternoon and early evening (approximately 3:05 pm to 6:20 pm). Following the transient, sleep-wake behavior re-entrains to the circadian rhythm, and the timing and duration of baseline sleep are re-established.

If a point is below the y = x -line, the time spent asleep (awake) is (in hours)

$$\Delta S = 24(1-x) + y. \tag{2.8}$$

In what follows, we show that these predictions for the duration of recovery sleep obtained from the map are consistent with both experimental data associated with 8- and 24-hours of sleep deprivation and our simulations of a range of sleep deprivations from 0- to 24-hours in the full sleep-wake model which incorporates features of sleep deprivation such as realistic patterns of light exposure and increases in homeostatic sleep drive above typical values (see Figs. 4 and 5).

3. Results

The one-dimensional sleep onset-to-sleep onset map Φ_{ss} (Fig. 3 A) represents the dynamics of the model for the sleep-wake regulatory network (see Section 2.1). The stable periodic solution is indicated by the fixed point of Φ_{ss} (sleep onset near 0.83 \approx at 11:58pm) corresponding to a typical human baseline sleep onset on the descending phase of the circadian cycle. The map Φ_{ss} also has an unstable fixed point (near 0.54 \approx 4:58pm) with a slope slightly larger than 1. A distinctive

feature of Φ_{SS} is the vertical discontinuity for initial sleep onsets occurring just past the circadian peak (0.5 $\leq \phi_n \leq$ 0.6). This discontinuity reflects a large increase in the phase (time) of succeeding sleep onsets for only small differences in the phase (time) of the initial sleep onsets [and is due to a tangency of the trajectory with the saddle-node bifurcation points of the steady state solution surface (Fig. 2B and D)].

The map Φ_{ss} also illustrates variations in the number of REM bouts per sleep episode depending on the circadian phase of sleep onset, with cusps over the interval $0.6 \le \phi_n \le 1$ demarcating the regions of the map associated with different characteristic numbers of REM bouts. For example, sleep onsets near the stable fixed point result in 4 REM bouts per sleep episode while sleep onsets at earlier and later phases (and past the respective cusps) contain 5 and 3 REM bouts, respectively. The decomposed maps Φ_{sw} and Φ_{ws} lack fixed points but maintain features of Φ_{ss} (Fig. 3C, D), such as the vertical discontinuity for wake onset phases in the interval (0.6,0.8) in Φ_{ws} (Fig. 3D) (which indicates that the discontinuity in Φ_{ss} near $\phi_n = 0.5$ is due to a discontinuous change in wake episode duration). The map Φ_{sw} (Fig. 3C) contains cusps that demarcate regions of Φ_{ss} associated with different numbers of REM bouts within the sleep episode.

Above all, Φ_{ss} can be used to approximate sleep-wake patterns of recovery sleep following sleep deprivation. As a result of sleep deprivation, sleep onset occurs at different circadian phases (times) and the evolution of model trajectories back to the stable sleep-wake solution represents recovery sleep and can be tracked on Φ_{ss} by the usual cobwebbing technique. For example, recovery from 8 and 20 h of sleep deprivation are indicated with cobwebbing in Fig. 3B where the asterisks show the sleep onset phases computed from the sleep deprivation simulations shown in Fig. 2.

Predictions for the length of recovery sleep computed from Φ_{ss} (using Eqs. (2.7)–(2.8), Fig. 4) indicate that sleep episodes starting 0–19 h after the usual sleep onset time result in shorter total and REM sleep durations compared to the baseline sleep. For longer periods of sleep deprivation, the map predicts a sharp increase in the duration of recovery sleep. This pattern agrees with results observed in human experimental data [1] and in simulations of the two-process model [3]. In addition, recovery sleep durations computed from Φ_{ss} are consistent with durations obtained from simulations of the full model (compare black dots with red crosses in Fig. 4) despite the inability of the map to account for the increases in homeostatic sleep drive H accrued during the deprivation period or the altered light conditions during extended wakefulness. Furthermore, both the map predictions and the sleep deprivation simulations for total sleep time and REM sleep time are consistent with experimental data for recovery following 8 and 20 h of sleep deprivation [28] (see blue dots and error bars in Fig. 4). The durations of total sleep and REM sleep during recovery show discrete jumps for increasing hours of sleep deprivation due to changes in the number of REM bouts, with the shortest sleep episodes containing 3 REM bouts and the longest sleep episodes containing 6 REM bouts.

A comparison between the map and sleep deprivation simulations shows that for the first recovery sleep episode (R1), the sleep durations predicted by Φ_{SS} differ by less than an hour (half an hour) for total (REM) sleep time from the model simulations for most sleep deprivation hours (see blue triangles in Fig. 5A and C). This suggests that the circadian effects on the duration of total sleep and REM sleep during recovery that are represented by the map dominate other factors contributing to the length of recovery sleep in the model. For most sleep deprivation hours, the map predictions agree with the simulations by the fifth recovery episode (R5, see yellow circles in Fig. 5A and C). However, for sleep onsets that occur 15–16 h past the usual sleep onset (i.e., during the afternoon and near the vertical gap of the map), the simulated solutions have not returned to the baseline sleep by the fifth recovery episode. The discrepancy between the map and model simulations is also larger for these (and nearby) sleep deprivation hours due to the large vertical gap in the map. These long-lasting effects of sleep deprivations of 15–16 h can be explained by the unstable fixed point on the map as illustrated in a representative sleep deprivation simulation where sleep onset phases remain in the region of the unstable fixed point of the map for many iterations (see Fig. 6A). Similarly, recovery sleep episodes simulated with the full model exhibit an approximately 12-day transient (during which sleep of about 4.3 h with 4 REM bouts occurs in the afternoon and early evening) before returning to the baseline (see Fig. 6B).

4. Conclusions

In this work, we applied a one-dimensional map describing the dynamics of an 8-dimensional, physiologically-based, ordinary differential equation model for human sleep-wake regulation to predict the effects of acute (i.e., one-time, less than 24-hour) sleep deprivation. The map reproduces patterns in the durations of recovery sleep observed in both experimental data and simulations of sleep deprivation using the full model. In addition, the accuracy of the predictions computed from the map suggests that the circadian rhythm and its influences are stronger than the effect of the homeostatic sleep drive on the duration of recovery sleep.

Although the map is a simplification of the sleep-wake regulation model, it helps to explain sleep deprivation simulations in three principal ways. First, the map describes the effects of circadian phase on the duration of recovery sleep and establishes a lower bound for recovery sleep durations. This is because the map does not account for additional aspects of sleep deprivation that would increase the duration of recovery sleep (such as increased homeostatic sleep drive and prolonged light exposure during sleep deprivation which are considered in the full sleep-wake model). Second, the map predicts that the duration of sleep deprivation, and the resulting circadian phase of the sleep onset, can affect the time course of recovery sleep over multiple days (which is consistent with simulation results using the full model). In particular, sleep onsets at circadian phases near the large, vertical discontinuity of the map (i.e., when $\phi_n = 0.5$ near the peak of the circadian rhythm) result in a long recovery to baseline sleep. Finally, cobwebbing on the map can be used to estimate and illustrate the evolu-

tion of sleep-wake behavior during recovery from sleep deprivation and return to the baseline sleep. Thus, the map provides a computationally-efficient tool for predicting features of recovery sleep that follows sleep deprivation.

Both total sleep and REM sleep time are increasingly recognized as important for cognitive performance and physical and mental health (e.g., [29–33]). This awareness has led to the development of multiple mobile applications and electronic monitoring systems that track sleep and promote healthy sleep habits (e.g., [34,35]). Many of these programs rely on mathematical models to predict sleep durations and responses to disrupted sleep schedules. We propose that one-dimensional maps can provide a computationally-efficient means to predict the effects of acute sleep deprivation. A map, such as the one presented here, that predicts the timing and duration of total and REM sleep during recovery sleep, may be leveraged to design optimal recovery strategies for individuals exposed to acute sleep deprivation. Moreover, these strategies may be designed to account for constraints such as limited recovery sleep time or repeated sleep deprivations. Previously, map-based approaches have been applied to represent entrainment of the circadian oscillator following perturbations such as transmeridian travel [36,37]. Thus, computationally-efficient representations of sleep and circadian dynamics may be used to simulate a range of sleep perturbation and recovery scenarios. However, inter-individual differences in baseline sleep may also affect responses to sleep deprivation [15,38] and jet lag [39]. Therefore, future work is needed to identify the key parameters necessary for representing interindividual variability in sleep-wake responses and, thereby, enable the derivation of maps that provide real-time, personalized predictions for recovery sleep.

Declaration of Competing Interest

The authors declare that they have no known competing financial interests or personal relationships that could have appeared to influence the work reported in this paper.

Acknowledgments

The authors acknowledge Grace O'Brien for her help creating 3D plots of model solutions and trajectories. This work was supported by the National Science Foundation under Grant Numbers DMS-1853506 (VB, SHP, CA) and DMS-1853511 (CDB). Any opinions, findings, and conclusions or recommendations expressed in this material are those of the author(s) and do not necessarily reflect the views of the National Science Foundation.

References

- [1] Akerstedt T, Gillberg M. The circadian variation of experimentally displaced sleep. Sleep 1981;4(2):159-69. doi:10.1093/sleep/4.2.159.
- [2] Rechtschaffen A, Bergmann BM, Gilliland MA, Bauer K. Effects of method, duration, and sleep stage on rebounds from sleep deprivation in the rat. Sleep 1999;22(1):11–31. doi:10.1093/sleep/22.1.11.
- [3] Daan S, Beersma D, Borbely A. Timing of human sleep: recovery process gated by a circadian pacemaker. Am J Physiol 1984;246:R161-83.
- [4] Postnova S, Layden A, Robinson PA, Phillips AJK, Abeysuriya RG. Exploring sleepiness and entrainment on permanent shift schedules in a physiologically based model. J Biol Rhythms 2012;27(1):91–102. doi:10.1177/0748730411419934.
- [5] Gordon CJ, Comas M, Postnova S, Miller CB, Roy D, Bartlett DJ, Grunstein RR. The effect of consecutive transmeridian flights on alertness, sleep-wake cycles and sleepiness: a case study. Chronobiol Int 2018;35(11):1471–80. doi:10.1080/07420528.2018.1493597.
- [6] Behn CGD, Kopell N, Brown EN, Mochizuki T, Scammell TE. Delayed orexin signaling consolidates wakefulness and sleep: physiology and modeling. J Neurophysiol 2008;99(6):3090-103. doi:10.1152/jn.01243.2007.
- [7] Behn CD, Booth V. Simulating microinjection experiments in a novel model of the rat sleep-wake regulatory network. J Neurophysiol 2010;103:1937-53.
- [8] Borbély AA. A two process model of sleep regulation. Hum Neurobiol 1982;1(3):195–204.
- [9] Mallis MM, Mejdal S, Nguyen TT, Dinges DF. Summary of the key features of seven biomathematical models of human fatigue and performance, Aviat Space Environ Med 2004;75(3):A4–A14.
- [10] Aeschbach D, Cajochen C, Landolt H, Borbely AA. Homeostatic sleep regulation in habitual short sleepers and long sleepers. Am J Physiol 1996;270(1):R41–53.
- [11] Kumar R, Bose A, Mallick B. A mathematical model towards understanding the mechanism of neuronal regulation of wake-NREMS-REMS states, PLoS One 2012;7:e2059.
- [12] Rempe M, Best J, Terman D. A mathematical model of the sleepwake cycle. J Math Biol 2010;60:615-44.
- [13] Postnova S, Lockley SW, Robinson PA. Prediction of cognitive performance and subjective sleepiness using a model of arousal dynamics. J Biol Rhythms 2018;33(2):203–18. doi:10.1177/0748730418758454.
- [14] Phillips AJK, Robinson PA. Sleep deprivation in a quantitative physiologically based model of the ascending arousal system. J Theor Biol 2008;255:413–23.
- [15] Piltz SH, Behn CGD, Booth V. Habitual sleep duration affects recovery from acute sleep deprivation: a modeling study. J Theor Biol 2020;504:110401. doi:10.1016/j.jtbi.2020.110401.
- [16] Nakao M, Yamamoto M. Bifurcation properties of the two process model. Psychiatry Clin Neurosci 1998;52(2):131-3.
- [17] Nakao M, Sakai H, Yamamoto M. An interpretation of the internal desynchronizations based on dynamics of the two-process model. Methods Inf Med 1997;36(04/05):282–5.
- [18] Skeldon A, Dijk D-J, Derks G. Mathematical models for sleep-wake dynamics: comparison of the two-process model and a mutual inhibition neuronal model. PLoS One 2014;9:e103877.
- [19] Bailey MP, Derks G, Skeldon AC. Circle maps with gaps: understanding the dynamics of the two-process model for sleep-wake regulation. Eur J Appl Math 2018:1–24.
- [20] Gleit RD, Behn CD, Booth V. Modeling interindividual differences in spontaneous internal desynchrony patterns. J Biol Rhythms 2013;28:339-55.
- [21] Booth V, Xique I, Behn CGD. One-dimensional map for the circadian modulation of sleep in a sleep-wake regulatory network model for human sleep. SIAM J App Dyn Systems 2017;16(2):1089–112.
- [22] Behn CD, Booth V. A fast-slow analysis of the dynamics of REM sleep. SIAM J App Dyn Systems 2012;11:212-42.
- [23] Forger DB, Jewett ME, Kronauer RE. A simpler model of the human circadian pacemaker. J Biol Rhythms 1999;14:532–7.
- [24] Kronauer RE, Forger DB, Jewett ME. Quantifying human circadian pacemaker response to brief, extended, and repeated light stimuli over the photopic range. J Biol Rhythms 1999;14:501–15.

- [25] Serkh K, Forger DB. Optimal schedules of light exposure for rapidly correcting circadian misalignment. PLoS Comput Biol 2014;10:e1003523.
- [26] Deboer T, M V, Detarii L, Meijer J. Sleep states alter activity of suprachiasmatic nucleus neurons. Nat Neurosci 2003;6:1086-90.
- [27] Rusterholz T, Durr R, Achermann P, Inter-individual differences in the dynamics of sleep homeostasis. SLEEP 2010;33:491-8.
- [28] Benoit O, Foret J, Bouard G, Merle B, Landau J, Marc ME. Habitual sleep length and patterns of recovery sleep after 24 h and 36 h sleep deprivation. Electroencephalogr ClinNeurophysiol 1980;50(5):477–85.
- [29] Knutson KL, Spiegel K, Penev P, Cauter EV. The metabolic consequences of sleep deprivation. Sleep Med Rev 2007;11(3):163-78. doi:10.1016/j.smrv. 2007.01.002.
- [30] Vogel GW. A review of REM sleep deprivation. Archives of General Psychiatry 1975;32(6):749-61. doi:10.1001/archpsyc.1975.01760240077006.
- [31] Song Y, Blackwell T, Yaffe K, Ancoli-Israel S, Redline S, Stone K. Relationships between sleep stages and changes in cognitive function in older men: the MrOS sleep study. Sleep 2015;38(3):411–21. doi:10.5665/sleep.4500.
- [32] Goldstein AN, Walker MP. The role of sleep in emotional brain function. Annual Review of Clinical Psychology 2014;10(1):679-708. doi:10.1146/annurev-clinpsy-032813-153716. PMID: 24499013
- [33] Simon SL, Behn CD, Cree-Green M, Kaar JL, Pyle L, Hawkins SM, Rahat H, Garcia-Reyes Y, Wright KP, Nadeau KJ. Too late and not enough: School year sleep duration, timing, and circadian misalignment are associated with reduced insulin sensitivity in adolescents with overweight/obesity. The Journal of Pediatrics 2019;205:257–64. doi:10.1016/j.jpeds.2018.10.027.
- [34] Walch OJ, Cochran A, Forger DB. A global quantification of "normal" sleep schedules using smartphone data. Science Advances 2016;2(5). doi:10.1126/sciadv.1501705.
- [35] Behar J, Roebuck A, Domingos JS, Gederi E, Clifford GD. sleep screening applications for smartphones. Physiol Meas 2013;34(7):R29-46. doi:10.1088/0967-3334/34/7/r29.
- [36] Diekman CO, Bose A. Entrainment maps: a new tool for understanding properties of circadian oscillator models. J Biol Rhythms 2016;31(6):598-616. doi:10.1177/0748730416662965.
- [37] Diekman CO, Bose A. Reentrainment of the circadian pacemaker during jet lag: east-west asymmetry and the effects of north-south travel. Journal of Theoretical Biology 2018;437:261–85. doi:10.1016/j.jtbi.2017.10.002.
- [38] Dongen HPAV, Vitellaro KM, Dinges DF. Individual differences in adult human sleep and wakefulness: leitmotif for a research agenda. Sleep 2005;28(4):479–98.
- [39] Ashkenazi IE, Reinberg AE, Motohashi Y. Interindividual differences in the flexibility of human temporal organization: pertinence to jet lag and shiftwork. Chronobiol Int 1997;14(2):99–113. doi:10.3109/07420529709001148.